Journal Pre-proof

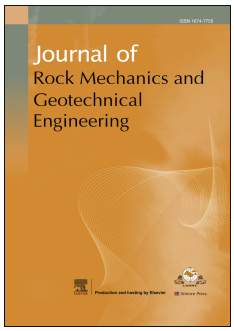

Biochar–water–soil interactions: Implications for soil desiccation cracking behavior in subtropical regions

Yu Lu, Kai Gu, Yuping Zhang, Zhengtao Shen, Chao-Sheng Tang, Qiyou Zhou, Bin Shi

PII: S1674-7755(24)00464-5

DOI: https://doi.org/10.1016/j.jrmge.2024.05.058

Reference: JRMGE 1767

To appear in: *Journal of Rock Mechanics and Geotechnical Engineering*

Received Date: 15 November 2023

Revised Date: 2 April 2024

Accepted Date: 28 May 2024

Please cite this article as: Lu Y, Gu K, Zhang Y, Shen Z, Tang C-S, Zhou Q, Shi B, Biochar–water–soil interactions: Implications for soil desiccation cracking behavior in subtropical regions, *Journal of Rock Mechanics and Geotechnical Engineering*, https://doi.org/10.1016/j.jrmge.2024.05.058.

Full Length Article

Biochar–water–soil interactions: Implications for soil desiccation cracking behavior in subtropical regions

Yu Lu[a], Kai Gu[a, b, *], Yuping Zhang[a, c], Zhengtao Shen[a], Chao-Sheng Tang[a], Qiyou Zhou[a], Bin Shi[a]

[a] School of Earth Sciences and Engineering, Nanjing University, Nanjing, 210023, China

[b] Frontiers Science Center for Critical Earth Material Cycling, Nanjing University, Nanjing, 210023, China

[c] Key Laboratory of Geohazard Prevention of Hilly Mountains, Ministry of Natural Resources, Geological Engineering Survey in Fujian Province, Fuzhou, 350003, China

*Corresponding author. E-mail address: gukai@nju.edu.cn

Abstract: In subtropical regions, soil desiccation cracking often exerts a significant impact on the interactions between soil water and the atmosphere, making it a subject of great interest in the fields of geotechnical and geoenvironmental engineering. Despite the growing utilization of biochar as a sustainable soil amendment, there remains a lack of in-depth understanding of biochar–water–soil interactions, as well as its impact on soil desiccation cracking behavior. To address this gap, this study investigated the influence and mechanism of woody biochar dosages and particle sizes on the cracking behavior of three typical clayey soils in subtropical regions in China, namely Pukou expansive soil (PKE), Xiashu soil (XS), and Zhongshan lateritic soil (ZSL). The quantitative analysis of crack images revealed that the use of biochar was not consistently effective in preventing soil cracking. The application of biochar reduced the crack ratio in PKE and XS by up to 24.03% and 53.89%, respectively. In contrast, ZSL exhibited a 74.57% increase in crack ratio with the addition of 10% biochar. This influence can be further enhanced by increasing the dosage and reducing the particle size of biochar. The microstructural analysis demonstrated that biochar exerts an inhibitory effect on PKE and XS primarily through direct replacement, direct barrier, and indirect physical mechanisms. Moreover, an indirect chemical effect between biochar and clay particles was proposed to explain the exacerbated cracking observed in biochar-amended ZSL. To effectively utilize biochar for soil cracking mitigation in subtropical regions, it is essential to evaluate the initial mineral composition and cation type of the soil.

Keywords: Biochar–water–soil interactions; Woody biochar; Desiccation cracking; Clayey soils; Influencing factors

1. Introduction

Drought is a highly destructive and costly natural disaster on a global scale. Its intensity, frequency, and periodicity have significantly increased in recent years due to climate change (Meehl and Tebaldi, 2004; Piao et al., 2010), especially in tropical and subtropical regions (Sherwood and Fu, 2014). In these subtropical regions of China, where clayey soils are commonly encountered, water loss through evaporation during drought can result in the formation of desiccation cracking. Cracks can significantly impact soil–water–atmosphere interactions and may give rise to various environmental issues (Morris et al., 1992; Lu, 2020; Yan et al., 2021; Cui, 2022). For example, clay barrier layers in nuclear disposal facilities and landfill covers necessitate low permeability. Cracking can enhance soil permeability and facilitate the migration of waste leachate into groundwater and landfill gas emission into the atmosphere, thereby compromising the efficacy and sealing capacity of clay barrier layers (Albrecht and Benson, 2001; Tang et al., 2019; Cheng et al., 2021). It is therefore evident that the mitigation of drought-induced soil cracking represents a significant engineering need in practice.

Among the various methods, that have been proposed, the utilization of biochar produced through the pyrolysis of biomass under limited or zero oxygen conditions has gained increasing attention. This is primarily due to the multifaceted benefits of biochar, which include waste reuse, enhanced crop yields, carbon sequestration, remediation of contaminated sites, and improvement of soil hydrological and engineering properties (Woolf et al., 2010; Garg et al., 2021; Lehmann et al., 2021; Shen et al., 2021; Guo et al., 2024). Furthermore, the efficacy of biochar in such applications is also influenced by desiccation cracking. It is therefore imperative to investigate the effect of biochar on soil cracking. Lu et al. (2014) conducted swell-shrinkage tests on expansive clayey soil and found that the addition of rice husk biochar decreased the coefficient of linear extensibility, indicating the potential for biochar to mitigate soil cracking. Subsequently, numerous studies have demonstrated the efficacy of using biochar for the mitigation of soil cracking (Bordoloi et al., 2018; Hussain et al., 2020; Zhang et al., 2020; Lu et al., 2021), particularly woody biochar, which showed the best inhibiting effect on desiccation cracking (Kumar et al., 2020).

However, despite the complexity of cracking in biochar-amended soils (BAS), which can be influenced by both soil and biochar properties, the majority of current research has tended to focus on singular factors. This research gap could have a significant impact on the large-scale field applications of biochar in subtropical regions, especially given the considerable variation in clayey soil properties across different locations within the same region, which can be

attributed to factors such as geography and climate conditions. For instance, lateritic soils in regions with high temperatures and abundant rainfall undergo extensive chemical weathering, resulting in unfavorable soil properties, such as low cation exchange capacity (CEC), low content of exchangeable low-valent cations (K^+, Na^+, Ca^{2+}, and Mg^{2+}), high alumina and exchangeable Al^{3+} content, and kaolin-based clay minerals (Xu et al., 2003; He et al., 2004; D'Angelo et al., 2014; Bai et al., 2023; Pierozan et al., 2023). By contrast, relatively mild chemical weathering permits the preservation of more ions in the expansive soil and Xiashu loess, which is typically rich in illite and montmorillonite and exhibits a high CEC. It is expected that biochar will exert a range of modifying effects on the desiccation cracking behavior of these clayey soils. Moreover, the impact of biochar on soil cracking may also be influenced by the characteristics of biochar, such as particle size and dosage. The theoretical premise is supported by the diverse alterations in soil microstructure following biochar addition, as soil microstructure significantly influences cracking behavior (Cheng et al., 2020; Lu et al., 2022; Wan et al., 2022). Therefore, this study aims to provide a comprehensive understanding of the impact of biochar on the desiccation cracking behavior of soils, considering various influencing factors.

Recent studies have also sought to elucidate the observed cracking behavior at the macroscopic level by investigating the microscopic mechanisms involved. For example, Bordoloi et al. (2018) demonstrated that biochar was effective in mitigating soil cracking due to its high water retention capacity. Based on scanning electron microscope (SEM) images, Zhang et al. (2020) found that woody biochar inhibited cracking by occupying the shrinkage space of two clayey soils. Yang et al. (2021) proposed that the mitigation of cracking in BAS may be associated with the compression of the bound water film. Puspanathan et al. (2022) suggested that the reduction in crack intensity factors was attributed to the filling of the shrinkage space, high water retention, low inherent thermal conductivity, and improvement in soil aggregate stability resulting from biochar. Furthermore, the effectiveness of biochar in mitigating soil cracking depends on its particle size (Lu et al., 2022; Puspanathan et al., 2022). To date, a comprehensive and unified understanding of the interactions between biochar, water, and soil, particularly concerning their influence on soil cracking behavior, remains lacking.

The primary aim of this study is to comprehensively investigate the interactions among biochar, water, and soil, and their implications for the desiccation cracking behavior of three typical subtropical clayey soils in China. For this purpose, woody biochar was incorporated into the soils at varying dosages and particle sizes. A series of evaporation experiments were conducted on saturated slurries to observe the process of crack development. The impact of biochar on soil cracking behavior under various influencing factors was subsequently elucidated

through proposed biochar-water-soil interactions. The outcomes of this study contribute to the understanding of biochar-water-soil interactions for engineering applications in subtropical regions.

2. Material and methods

2.1. Experimental materials

Woody biochar was used in this study due to its better performance in mitigating soil cracking (Kumar et al., 2020). The biochar was produced through pyrolysis at 500 °C for 5h, and its physical and chemical properties are summarized in Table 1. Prior to the experiment, the biochar was oven-dried, crushed, and sieved into three distinct particle size classes: fine particles (< 0.25 mm), medium particles (0.25–1 mm), and coarse particles (1–2 mm). The biochar particles are elongated or flattened in shape, with sharp edges and corners (Lu et al., 2022). Irrespective of particle size, biochar exhibits a honeycomb structure with internal pores ranging from 5 μm to 20 μm in diameter (Fig. A1 in Appendix). This indicates that the woody biochar used in this study is a macroporous carbon material, which is consistent with the results of the specific surface area detected using the N_2 adsorption method (0.017–0.48 m^2/g for coarse to fine biochar).

Table 1
Basic properties of soils and biochar.

Pyrolysis temperature (°C)		Pyrolysis time (h)	Ash content (%)		pH	Bulk density (g/cm^3)	C (%)	H (%)	N (%)
500		5	28.26		10.28	0.47	78.01	3.55	0.22
Soil	Specific gravity	Grain size analysis (%)			Atterberg limits (%)			USCS classification (ASTM–2487, 2017)	
		Sand	Silt	Clay	Liquid limit	Plastic limit	Plastic index		
PKE	2.71	24.4	33.6	42.0	76.0	29.0	47.0	CH	
XS	2.72	6.3	69.5	24.2	36.2	18.8	17.4	CL	
ZSL	2.74	46.9	28.2	24.9	50.2	25.3	24.9	CH	

Subtropical regions are typically characterized by a warm and humid climate, with high temperatures and abundant rainfall. These conditions facilitate the weathering and decomposition of rocks and minerals, leading to the formation of clay particles. This study focuses on three typical clayey soils: Pukou expansive soil (PKE), Xiashu soil (XS), and Zhongshan lateritic soil (ZSL), which are widely distributed in subtropical regions of China (Fig. 1). X-ray diffraction analysis revealed that the clay component of PKE was primarily composed of illite (73.6%), montmorillonite (17.9%), and kaolinite (8.5%) (Gu et al., 2014). XS mainly consisted of non-clay minerals such as quartz and feldspar (65%), with illite (14%) and kaolinite (10%) being the dominant clay minerals. In contrast, ZSL was predominantly composed of kaolinite (66%)

and quartz (29%). Additional physical parameters of three soils are presented in Table 1. The raw soils were oven-dried, crushed, and passed through a sieve with a mesh size of < 0.25 mm for further use.

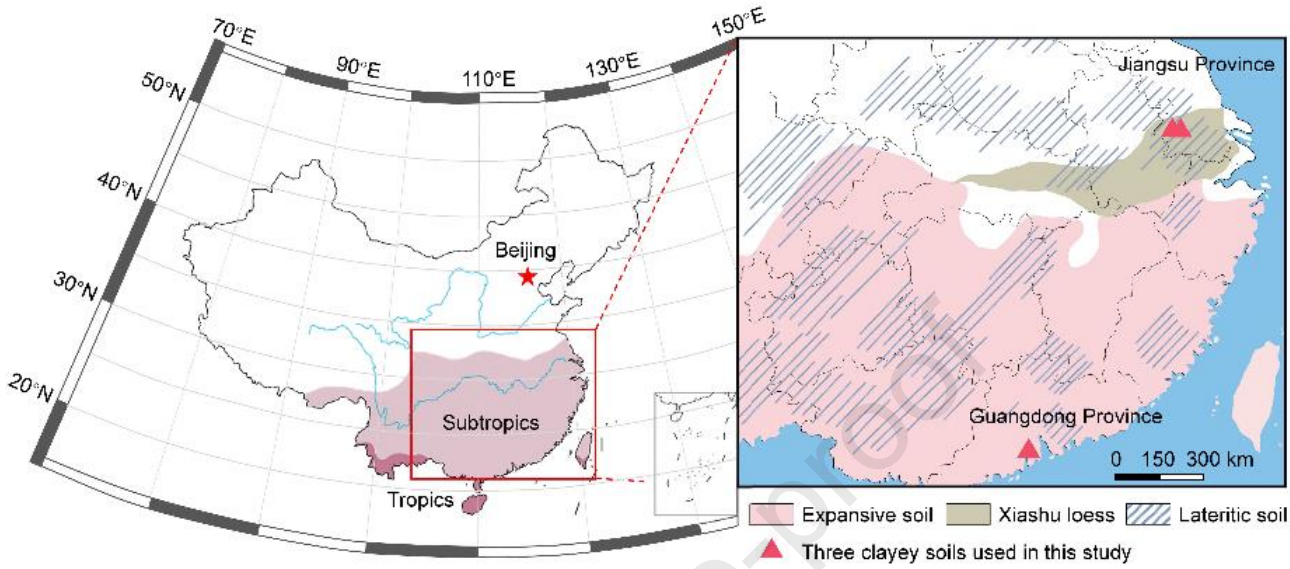

Fig. 1. Geographical location and geological conditions of subtropic and tropic regions in China (the distribution of expansive soil, Xiashu loess, and lateritic soil is obtained from Shi et al. (2002), Yan et al. (2014), and Hu et al. (2010), respectively).

2.2. Sample preparation and test apparatus

To achieve a uniform state, saturated slurries with an initial gravimetric water content of about 100% for PKE and 80% for XS and ZSL were employed, as previously described in the literature (Zhang et al., 2020; Lu et al., 2021). Prior to this, biochar was thoroughly mixed with soil in a dry state at selected dosages of 0%, 1%, 3%, 5%, and 10% (w/w), based on previous studies in the field of geotechnical and geoenvironmental engineering (Garg et al, 2021; Lu et al., 2022; Wan et al., 2022). Subsequently, the saturated slurries were sealed in plastic drums for a period of 48 h to ensure a homogeneous distribution of moisture. Thereafter, the samples were stirred for a further 10 min before being poured into plexiglass containers with a length and width of 20 cm. The sidewalls of the container were coated with vaseline to facilitate the detachment of the samples from the container sidewalls during shrinkage. Air bubbles present in the sample were carefully removed by vibrating the container, and the sample height was maintained at about 1 cm. Samples were named based on the particle size, soil type, and biochar dosage (Table 2). A total of 21 sets of tests were conducted, each in duplicate.

Table 2
Details of the experimental information.

Soil	Sample ID	Biochar dosage (%)	Biochar particle size (mm)

PKE	FPKE0-10	0, 1, 3, 5, 10	< 0.25
	MPKE3	3	0.25–1
	CPKE3	3	1–2
XS	FXS0-10	0, 1, 3, 5, 10	< 0.25
	MXS3	3	0.25–1
	CXS3	3	1–2
ZSL	FZSL0-10	0, 1, 3, 5, 10	< 0.25
	MZSL3	3	0.25–1
	CZSL3	3	1–2

After preparation, all samples were air-dried at a constant temperature of about 25 °C. Each sample was weighed and photographed at regular intervals to record the water content and crack development over a drying period of about 10 d. Desiccation cracking tests were completed when the change in sample mass was less than 0.01 g in two adjacent monitoring points.

Subsequently, small clods (with dimensions of approximately 0.5 cm × 0.5 cm × 2 cm) were prepared at the edges of cracks for SEM and mercury intrusion porosimetry (MIP) tests to explore the effect of biochar on the microstructure of soils. Prior to SEM and MIP tests, the freezing-drying method was employed (Delage et al., 1996). Selected small clods were frozen using liquid nitrogen and transferred into a freeze-dryer to obtain dried samples with a preserved microstructure.

2.3. Crack network quantification

Soil crack images were quantitatively analyzed using the software Crack Image Analysis System (CIAS). To minimize boundary effects on crack observations, the shrinkage region was excluded from the calculation of the crack ratio. Furthermore, to maximize the area used for calculating the crack ratio, the central portion of the images (18 cm × 18 cm) was ultimately retained for further analysis (see Fig. A2 in the Appendix). This area was selected based on the results of PKE, which exhibited the most pronounced shrinkage. The image processing procedures depicted in Fig. 2 comprised several steps: grayscale, binarization, denoising, skeletonization, and crack identification. The objective of these steps was to differentiate between cracks and clods. A crack segment is defined as the portion of a crack between two intersections where cracks intersect (Fig. 2). It is a measurable length. The width of the crack segment is calculated as the shortest distance from a random point on one boundary to the opposite boundary. In cases where two crack segments share an intersection point, the angle between them is referred to as the crack intersection angle. The surface crack ratio is calculated by dividing the surface area of all crack segments by the total area of the soil samples. Subsequently, a quantitative analysis of the geometrical parameters (e.g. surface crack ratio (R_{scr}), number of crack segments (N_{seg}), total length of cracks (L_{sum}), and average width of cracks

(W_{ave})) and statistical indices (e.g. the relative frequency of crack intersection angle) in soil samples was conducted by integrating the parameters of individual crack segments. More details regarding the description of crack parameters can be found in Tang et al. (2008) and Liu et al. (2013).

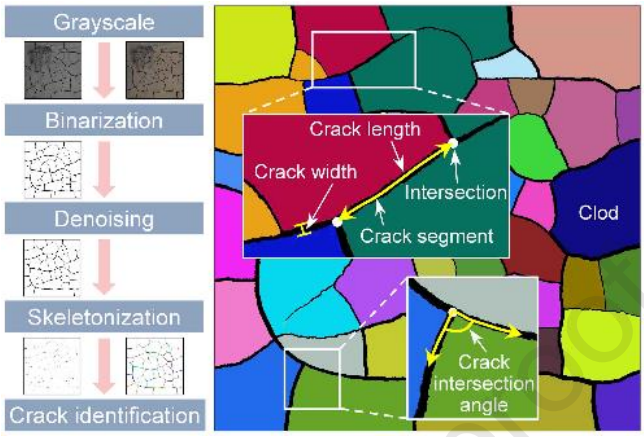

Fig. 2. Crack image processing procedures.

3. Results and discussion

3.1. Effect of soil types

Before investigating the effect of biochar on different clayey soils, it is necessary to clarify the desiccation cracking behavior of bare soils. Fig. 3 shows the process of crack initiation and propagation. As depicted in Fig. 3a and c, desiccation cracks developed sequentially in PKE and XS. The primary cracks appeared first (stage I), followed by sub-cracks perpendicular to the primary cracks (stage II). Primary and sub-cracks can be distinguished by final crack images, with the former being wider than the latter. Subsequently, the crack network tended to stabilize, with widening representing the predominant phenomenon (stage III). In contrast, ZSL exhibited a simultaneous generation of cracks at multiple locations on the sample surface, which then widened gradually, making it difficult to distinguish between primary and sub-cracks (Fig. 3e). The final crack morphology indicated that clods of PKE and XS were split into separate, nearly quadrangular or pentagonal shapes by smooth cracks, which generally developed in a T-shape. In contrast, cracks in ZSL were Y-shaped, with jagged crack segments, and most of them failed to completely penetrate the sample surface, resulting in crack networks with poor connectivity and clods of varying shapes. This can be explained by their different microstructure (Cheng et al., 2020; Tian et al., 2022). The pore size distribution (PSD) of PKE and XS shows an unimodal form (Fig. 4), indicative of a homogeneous microstructure dominated by intra-aggregate pores (micropores). Therefore, the concentration/release of strain energy and the generation of

desiccation cracks can be maintained in an orderly manner (Tang et al., 2008), leading to the T-shaped intersection angle (90°) between the primary and sub-cracks (Fig. 3a and c). In contrast, a bimodal PSD curve, typically observed in compacted soils on the dry side and optimum (Delage et al., 1996; Cheng et al., 2020), was evident in the ZSL samples (Fig. 4). The inter-aggregate pores (macropores) in soils can act as weak zones, inducing cracks to be initiated at multiple locations. Meanwhile, cracks intended to intersect at 120° (Y-shaped) macroscopically to follow the criterion of the most efficient use of energy, where the cracks will take the shortest path to expend the same amount of energy (Costa et al., 2013; Tian et al., 2022).

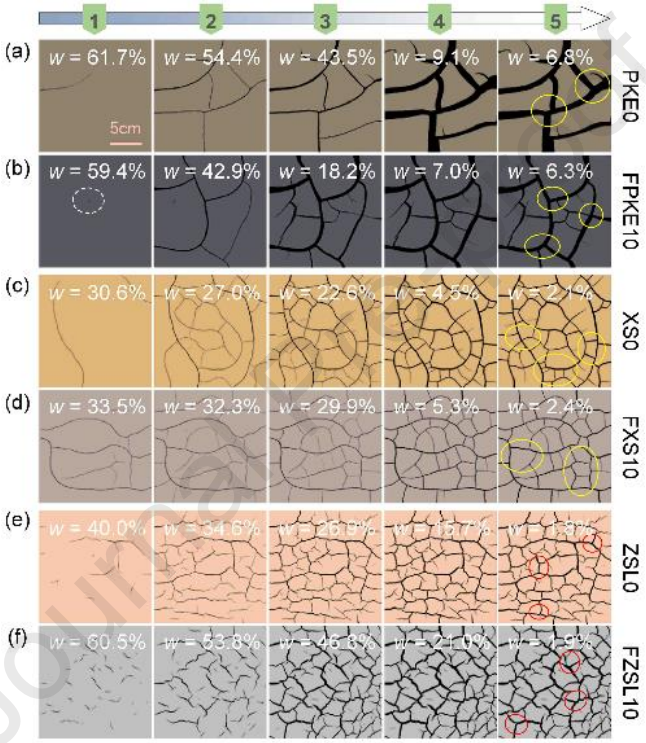

Fig. 3. Crack initiation and propagation process of BAS during drying: (a, b) PKE; (c, d) XS; and (e, f) ZSL. Stages I, II, and III occurred during the periods of 1–2, 2–3, and 3–5, respectively. The yellow and red circles represent the T- and Y-shaped cracks, respectively.

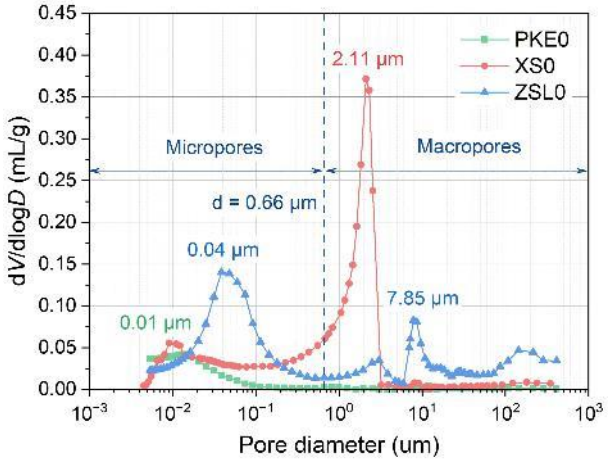

Fig. 4. PSD curves of three clayey soils.

Subsequently, a quantitative parameter analysis was performed using the CIAS, as illustrated in Fig. 5. The results demonstrated that during the drying process, the surface crack ratio (R_{scr}) and the average width of cracks (W_{ave}) of PKE exhibited a relatively constant rate of increase with the reduction in water content (Fig. 5a and b). A comparison of the crack parameters at different stages of crack development revealed that R_{scr} and W_{ave} primarily increased in stage III. Conversely, for XS and ZSL, the propagation velocity of R_{scr} and W_{ave} decreased significantly once the crack network was stabilized (Fig. 5c–f), and most of the crack parameters were completed before stage III. Furthermore, the sequence in which the crack parameters were completed before stage III was as follows: ZSL > XS > PKE. This indicates that the crack parameters of stages I and II are predominantly influenced by the crack length, with ZSL exhibiting the longest lengths and PKE displaying the shortest (Fig. 3). With regard to R_{scr} and W_{ave} at stage III (Fig. 5), PKE had the highest values due to its highest clay content, while the lowest values in ZSL were attributable to the prevalence of kaolinite clay minerals, despite the clay content of ZSL and XS being comparable.

The addition of biochar to different clayey soils was anticipated to elicit disparate outcomes with respect to desiccation cracking behavior. Although fine biochar did not change the pattern of crack development in any of the soils, it altered the process of crack initiation and propagation (Fig. 3). For PKE and ZSL, the development period of primary and sub-cracks was prolonged by biochar (Fig. 3b and f), and the increase in R_{scr} and W_{ave} was observed to occur primarily in stages I and II, rather than stage III (Fig. 5a and b). A quantitative analysis showed that, under the same water content, the R_{scr} and W_{ave} values were diminished in the biochar-amended PKE due to its lower crack propagation velocity, except in stage I, where the curve shape was similar (Fig. 5a and b). Therefore, biochar can inhibit the desiccation cracking of PKE during stages II and III. For XS, the water content at which cracks first appeared was increased after biochar addition (Fig. 3c and d). However, the relationship between R_{scr} and W_{ave} and water content during stage I was also similar (Fig. 5c and d). As the cracks developed to stages II and III, the variation of R_{scr} and W_{ave} with water content decreased gradually with the addition of biochar. This behavior caused the biochar to act as an inhibitor of soil cracking in stage III. In contrast, the curves for ZSL with biochar exhibited similar patterns during stage I, as well as stages II and III (Fig. 5e and f). Therefore, the high cracking water content resulted in higher crack parameters in biochar-amended ZSL than in bare soil at a given water content.

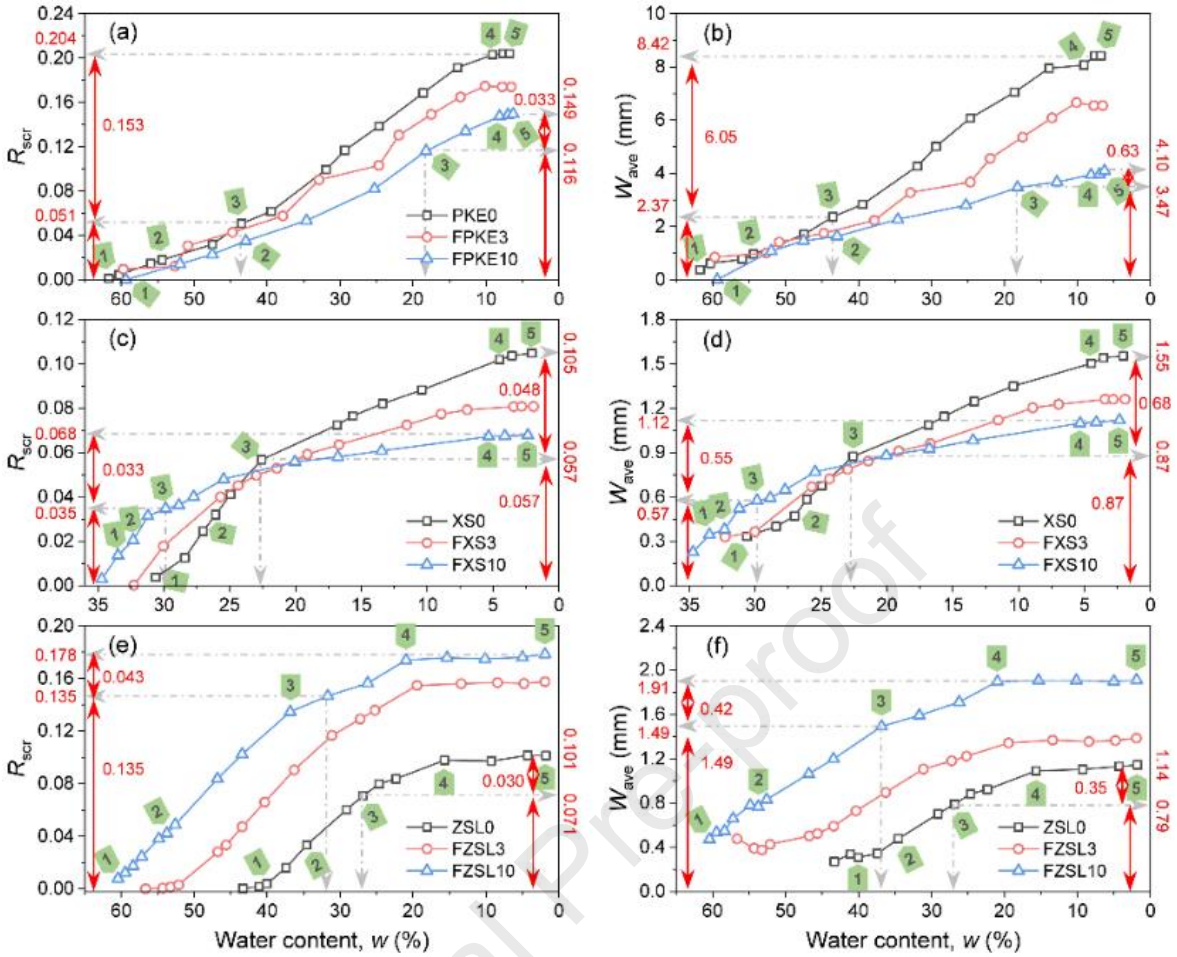

Fig. 5. The evolution of surface crack ratio (R_{scr}) and average width of cracks (W_{ave}) of soils during drying: (a, b) PKE; (c, d) XS; and (e, f) ZSL. Stage I, II, and III occurred during the periods of 1–2, 2–3, and 3–5, respectively.

Biochar has a significant effect on soil microstructure (Wong et al., 2018; Zhang et al., 2020; Lu et al., 2023), and further influences the processes of crack initiation and propagation (Lu et al., 2022). Fig. 6 shows the SEM images of the fine BAS. As illustrated in the figure, PKE had a dense structure with fewer developed micropores, while XS exhibited a relatively loose structure with larger micropores. In contrast, the structure of ZSL was the loosest, with a considerable range of pore sizes, including both macropores and micropores. These findings were consistent with those presented in Fig. 4. Notably, when biochar was added, microcracks that developed along the edges of biochar were observed in PKE (Fig. 6), thereby confirming our previous argument that biochar induces the development of cracks along their edges (Lu et al., 2021). Furthermore, regardless of soil type, biochar particles were tightly packed between the soil particles, and clay particles could partially clog the intra pores of biochar (Fig. 6, referred to as the barrier effect of biochar). In contrast to sand particles, biochar surfaces typically carry a negative charge, which increases the repulsive forces among clay particles that also possess negative charges. Meanwhile, the shrinkage of clay particles within the pores of biochar does not contribute to cracking. This, in conjunction with the direct partial replacement of soil particles

by biochar (collectively referred to as the direct effect of biochar), restricts the shrinkage of soil particles and partially elucidates the mitigated cracking observed in PKE and XS. Previous studies have identified a negative correlation between soil engineering properties and crack parameters (Tang et al., 2020; Cheng et al., 2021; Zhang et al., 2024). This suggests that biochar has the potential to mitigate engineering issues arising from increased infiltration and reduced strength. Consequently, it could be employed in geotechnical and geoenvironmental engineering applications, such as the use of biochar as a clay barrier layer in landfill final covers and topsoil in both bare and vegetated slopes.

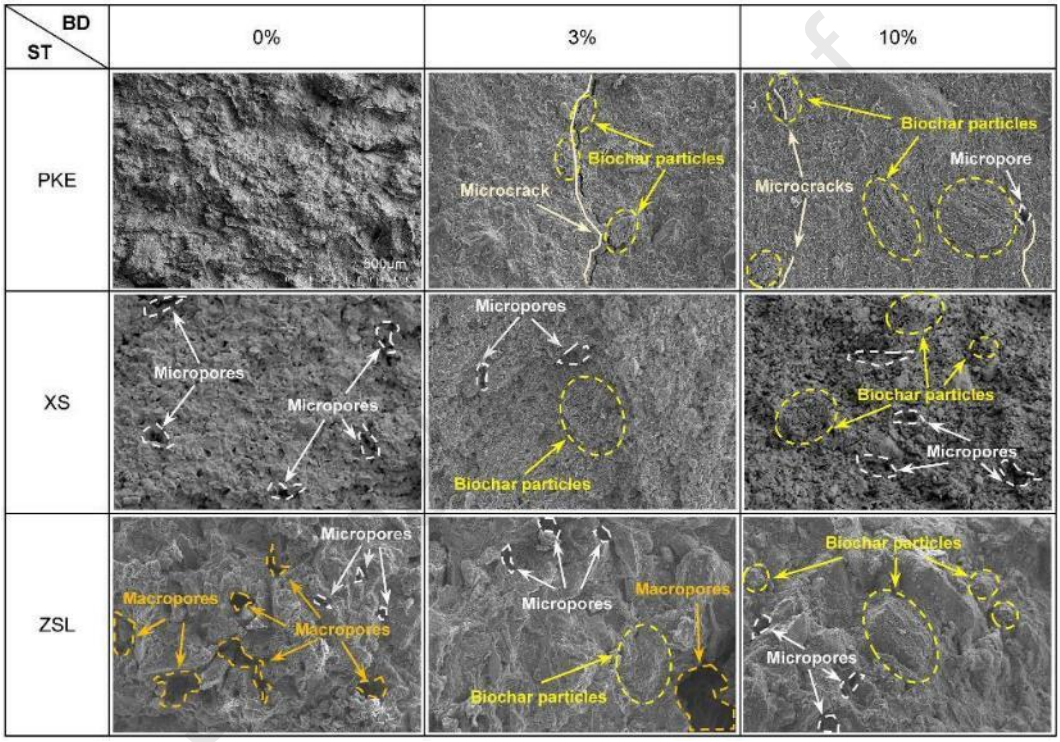

Fig. 6. SEM images of fine BAS. BD: Biochar dosage; ST: Soil type.

As for ZSL, the aggravated cracking by biochar may be attributed to the fact that biochar changes the thickness of the bound water film around clay particles. Most base elements (K^+, Na^+, Ca^{2+}, and Mg^{2+}) present in ZSL have been leached out due to intense weathering imposed by tropical and subtropical climates, and the cations are dominated by exchangeable Al^{3+} (Xu et al., 2003). The addition of woody biochar with abundant cations could increase the low-valent cations (e.g. K^+, Na^+, Ca^{2+}, and Mg^{2+}) present in weathered soils (Laird et al., 2010; Jien and Wang, 2013). This process of ion exchange between biochar and clay particles is referred to as the indirect chemical effect of biochar. In this process, biochar can partially replace Al^{3+} in ZSL (mainly kaolin) with low-valent cations, which could consequently increase the bound water film around clay particles. This assumption was supported by the consistency limits of ZSL, where both the liquid limit and the plasticity index were increased with increasing biochar

dosage (Fig. 7b). As a result, the indirect chemical effect overcomes the direct inhibitory effect mentioned above and aggravates soil cracking in ZSL, as observed macroscopically (Figs. 3e, f, 5e, and f). However, a moderate weathering intensity permits the preservation of more low-valent cations in XS (mainly illite). The lower ion exchange capacity between biochar and clay particles means that biochar has no significant impact on the liquid limit and plasticity index of the soil (Lu et al., 2022). The direct inhibitory effect remains dominant. In the case of PKE, its clay minerals are abundant in both illite and montmorillonite. This results in PKE having the highest liquid limit and plasticity index. The addition of biochar caused a notable reduction in these values (Fig. 7a). This implies that biochar diminishes the bound water film around clay particles, thus facilitating the mitigation of cracking. Consequently, the indirect chemical effect of biochar on soil cracking varies among the three clayey soils: it inhibits cracking in PKE, has a negligible effect in XS, and promotes cracking in ZSL.

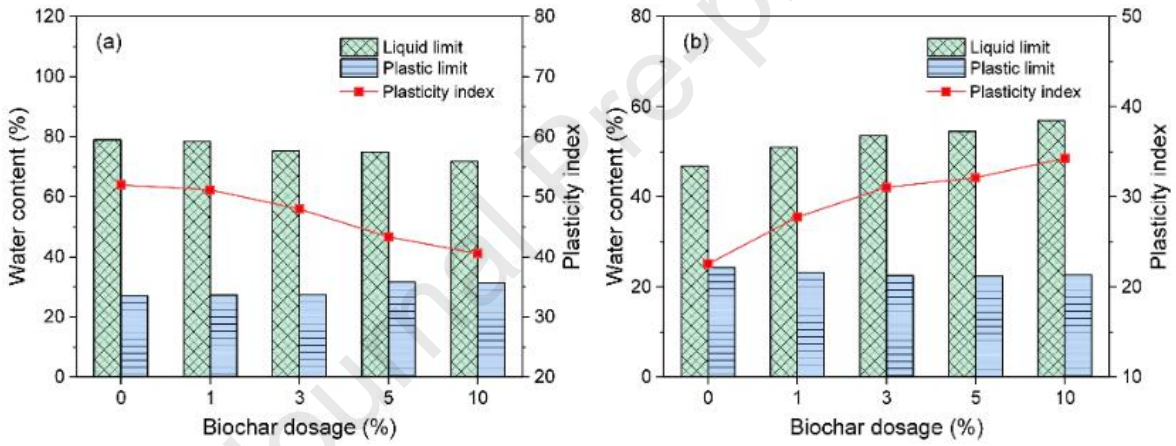

Fig. 7. Consistency limits of fine BAS: (a) PKE; and (b) ZSL.

Furthermore, the aforementioned theory can be used to explain the processes of crack initiation and propagation. During the process of drying, soil undergoes shrinking accompanied by water loss. When the tensile stress induced by capillary suction exceeded the tensile strength of the soil (Tang et al., 2010; Shin and Santamarina, 2011), cracks were initiated. The elevated cracking water content in biochar-amended XS was attributed to the extra water held by biochar (Lu et al., 2022) and the reduced tensile strength (Blanco-Canqui, 2021; Yang and Lu, 2021). However, this effect was counterbalanced by the reduced bound water film in PKE. In ZSL, the increased bound water film causes the soil to develop suction earlier, resulting in a more pronounced increase in cracking water content than in XS. It should be noted that soils remain saturated when cracking (Peron et al., 2009), and have sufficient space for shrinkage. The addition of biochar did not affect the early stage of crack parameter development (Lu et al., 2021). As cracks propagate, the pore space continues to decrease, and biochar gradually

demonstrates its ability to inhibit the shrinkage of PKE and XS. However, in ZSL, the dominance of the indirect chemical effect increased the bound water film around clay particles, allowing the curve pattern of crack ratio and average width of cracks to maintain its original shape. Therefore, it is essential to exercise caution when utilizing biochar to modify soil cracking behavior and related engineering properties in subtropical regions.

3.2. Effect of biochar dosages

The effect of biochar on the initiation and propagation of cracks increased with the increasing biochar dosage, as shown in Fig. 5. When the evaporation process has reached a state of equilibrium, the final crack morphology of BAS with various dosages is illustrated in Fig. A3 in the Appendix, and the quantitative parameters are plotted in Fig. 8. For PKE, as biochar dosage increased, R_{scr} firstly increased insignificantly and then stabilized in the range of 0.16–0.18, which was lower than that observed in the bare soil (Fig. 8a). N_{seg} and L_{sum} were the smallest with 3% biochar, which decreased by 34.48%, and 3.71%, respectively (Fig. 8b and c). The addition of more biochar will result in a further increase in these crack parameters. As for W_{ave}, a larger reduction was achieved in soils containing more biochar, reaching a maximum at 53.91% (Fig. 8d). For XS, all crack parameters showed a monotonically decreasing trend with increasing biochar dosage (Fig. 8). The greatest reduction was observed in samples with 10% biochar addition, with ratios of 39.57%, 31.01%, 14.51%, and 30.59% for R_{scr}, N_{seg}, L_{sum}, and W_{ave}, respectively. Similarly, R_{scr} and W_{ave} in ZSL increased monotonically when biochar was added, with an increase of 74.57% and 72.19%, respectively, at 10% biochar dosage (Fig. 8a and d). On the other hand, N_{seg} and L_{sum} increased initially and then decreased with increasing biochar dosage, but remained higher than the bare soil (Fig. 8b and c). The highest value was observed at 3% dosage, with a 37.80% and 17.49% increase compared to the bare soil.

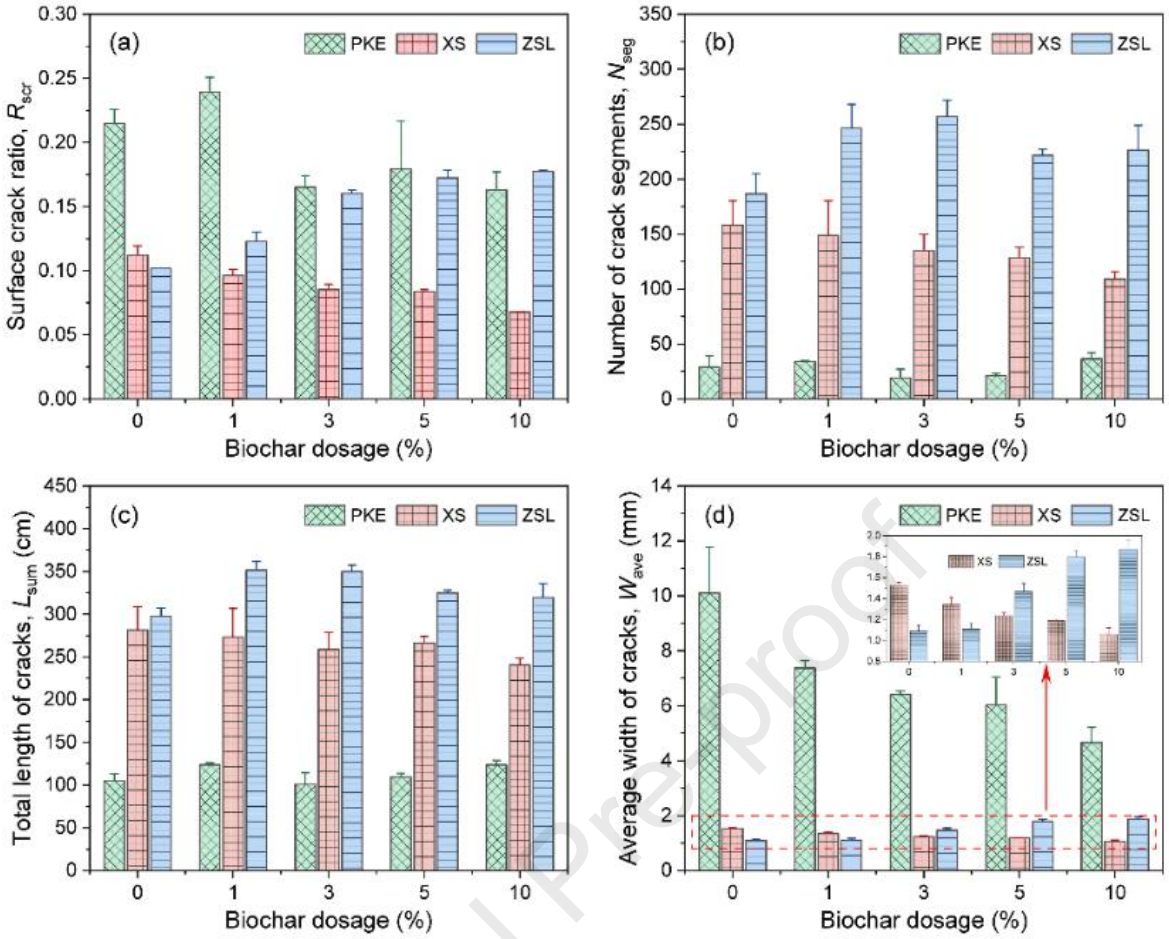

Fig. 8. Quantitative crack parameters of soils with varying biochar dosage: (a) Surface crack ratio, R_{scr}; (b) Number of crack segments, N_{seg}; (c) Total length of cracks, L_{sum}; and (d) Average width of cracks, W_{ave}.

Based on the theory presented in the previous section, the addition of more biochar may result in enhanced direct replacement and barrier effects, as well as indirect chemical influences, thereby conferring a more pronounced inhibitory impact on PKE. However, a similar reduction in R_{scr} was observed in 3% and 10% fine biochar-amended PKE, which may have been attributable to alterations in pore size (referred to as the indirect physical effect of biochar). As illustrated in Fig. 9, the unimodal PSD of PKE remained unaltered by the addition of 3% fine biochar, with a slight increase observed in the peak aperture size. The inhibitory effect results in a reduction of crack parameters. As the biochar dosage continued to increase, the presence of macropores in the 10% biochar-amended PKE permitted the generation of more cracks, resulting in longer crack lengths, narrower crack widths, and an insignificant change in surface crack ratio. For XS, the addition of fine biochar had no significant effect on the PSD curve (Fig. 9). The direct effect of biochar resulted in a more pronounced reduction in crack parameters of XS with increasing biochar dosage (Fig. 8). On the other hand, increasing the biochar dosage in ZSL was expected to enhance the indirect chemical effect between biochar and clay particles, thereby influencing the crack parameters. Additionally, the enhanced homogeneity resulting from a high

dosage of biochar enables stresses to be generated at reduced location (Fig. 6), leading to a further decrease in the number and length of cracks.

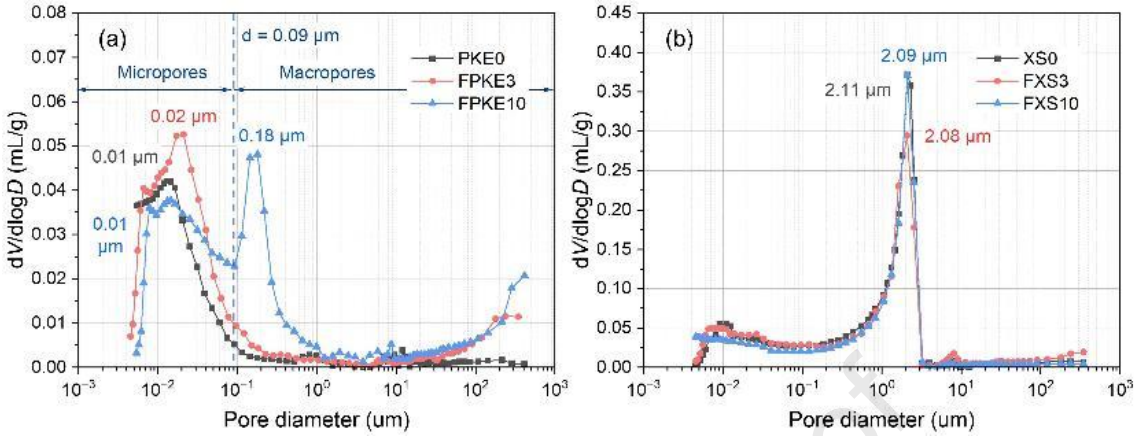

Fig. 9. PSD curves of fine BAS: (a) PKE; (b) XS.

It is therefore recommended that the selection of an appropriate biochar dosage should be based on soil properties, rather than assuming that a higher dosage will always be more beneficial, although this is often the case. For PKE, it is recommended to use a biochar dosage of 3%, considering the variations in all crack parameters. While the influence of biochar on XS and ZSL generally increases with higher dosages, this also leads to higher costs. It is therefore necessary to carefully consider the balance between the modifying effect and the costs of materials before applying biochar in subtropical regions.

3.3. Effect of biochar particle sizes

The processes of crack initiation and propagation in soils with varying particle sizes are different since desiccation cracks no longer develop sequentially, especially for CPKE and CXS. Fig. A4 in the Appendix presents the final crack patterns observed in soils with varying biochar particle sizes. For PKE and XS, more jagged Y-shaped cracks were observed as the biochar particle size increased, which differed from that in FPKE and FXS, where cracks with smooth segments intersect at 90°. In contrast, increasing biochar particle sizes failed to change the crack patterns of ZSL, and the Y-shaped crack intersection angle remained dominant.

The crack morphology of BAS can also be characterized in terms of quantitative parameters, such as the crack intersection angle. Fig. 10 shows the relative frequency of crack intersection angles for soils with various biochar particle sizes. For FPKE, crack intersection angles are mainly concentrated within the range of 80°–100° (Fig. 10a), corresponding to T-shaped cracks that developed sequentially (Fig. 3a). As biochar particle sizes increase, the relative frequency of the intersection angle between 110° and 140° gradually increases and dominates in CPKE (Fig. 10b and c). This indicates that the process of crack initiation and propagation has undergone a

transformation from a sequential to a simultaneous development. A similar observation was made in XS (Fig. 10d–f). However, the effect of biochar particle sizes on the crack intersection angle is less pronounced than that of PKE. In ZSL, the crack intersection angle always remains dominated by 110°-140°, regardless of biochar particle sizes (Fig. 10h–j). Therefore, variations in the relative frequency of crack intersection angles resulting from biochar particle size will inevitably influence the ultimate crack parameters.

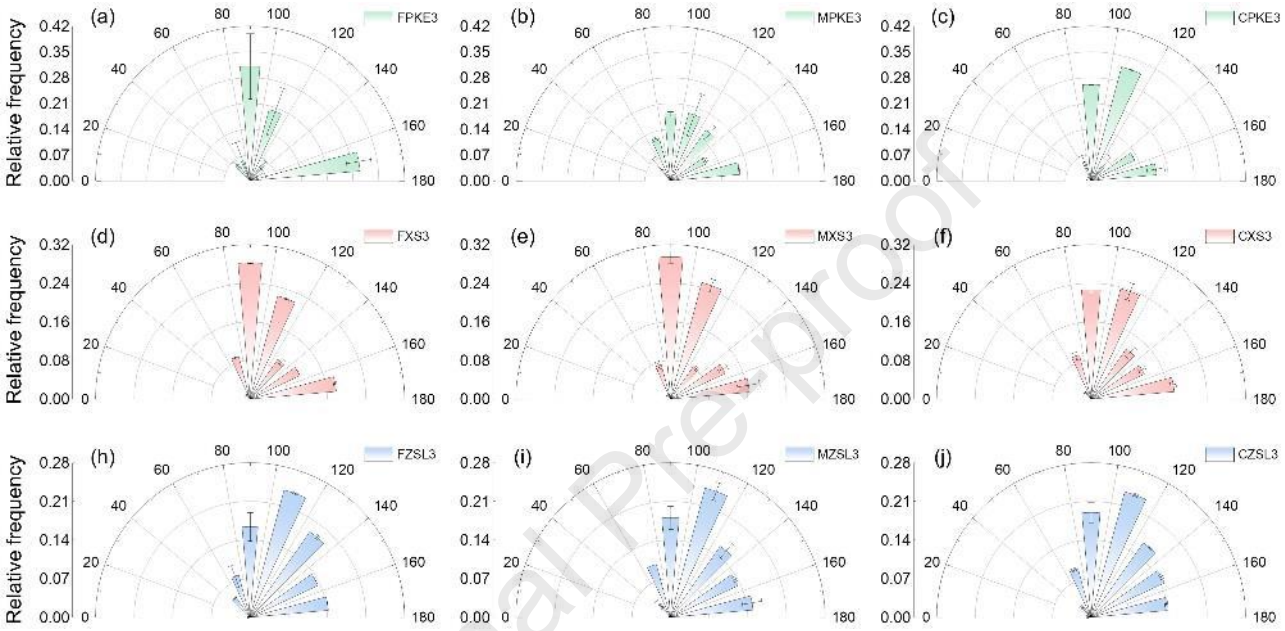

Fig. 10. The relative frequency of crack intersection angle for samples with various biochar particle sizes: (a)–c) PKE; (d–f) XS; and (h–j) ZSL.

The quantification analysis of the crack parameters is shown in Fig. 11. The effect of biochar particle size on desiccation cracking differs significantly between PKE, XS, and ZSL, as is the case with different biochar dosages. In PKE and XS, crack parameters except W_{ave} increased with increasing biochar particle size (Figs. 11a-c). Compared to bare soil, biochar with medium and coarse particle sizes weakens its inhibitory effect on soil cracking by promoting the formation of cracks. For example, the R_{scr} of FPKE3, MPKE3, and CPKE3 was reduced by 23.13%, 16.93%, and 6.67%, respectively, while the N_{seg} and L_{sum} of MPKE3 and CPKE3 were increased by 3.45%, 6.97%, and 55.17%, 30.32%, respectively. Conversely, cracks became progressively narrower as the biochar particle size increased, and coarse biochar-amended PKE and XS had the most significant reduction in crack width, reaching 44.38% and 39.13%, respectively (Fig. 11d). In comparison, for ZSL, all crack parameters tended to decrease with increasing biochar particle size (Fig. 11). The R_{scr}, N_{seg}, L_{sum}, and W_{ave} of samples amended with coarse biochar decreased by 21.16%, 29.77%, 18.06%, and 2.96%, respectively, compared to those amended with fine biochar. However, there was still a 24.24% and 30.91% increase in W_{ave} and R_{scr} observed

compared to the bare soil, although N_{seg} and L_{sum} increased insignificantly. Overall, the findings suggest that increasing the particle size of biochar weakened its inhibitory effect on desiccation cracking in PKE and XS, while also reducing its promotion effect in ZSL.

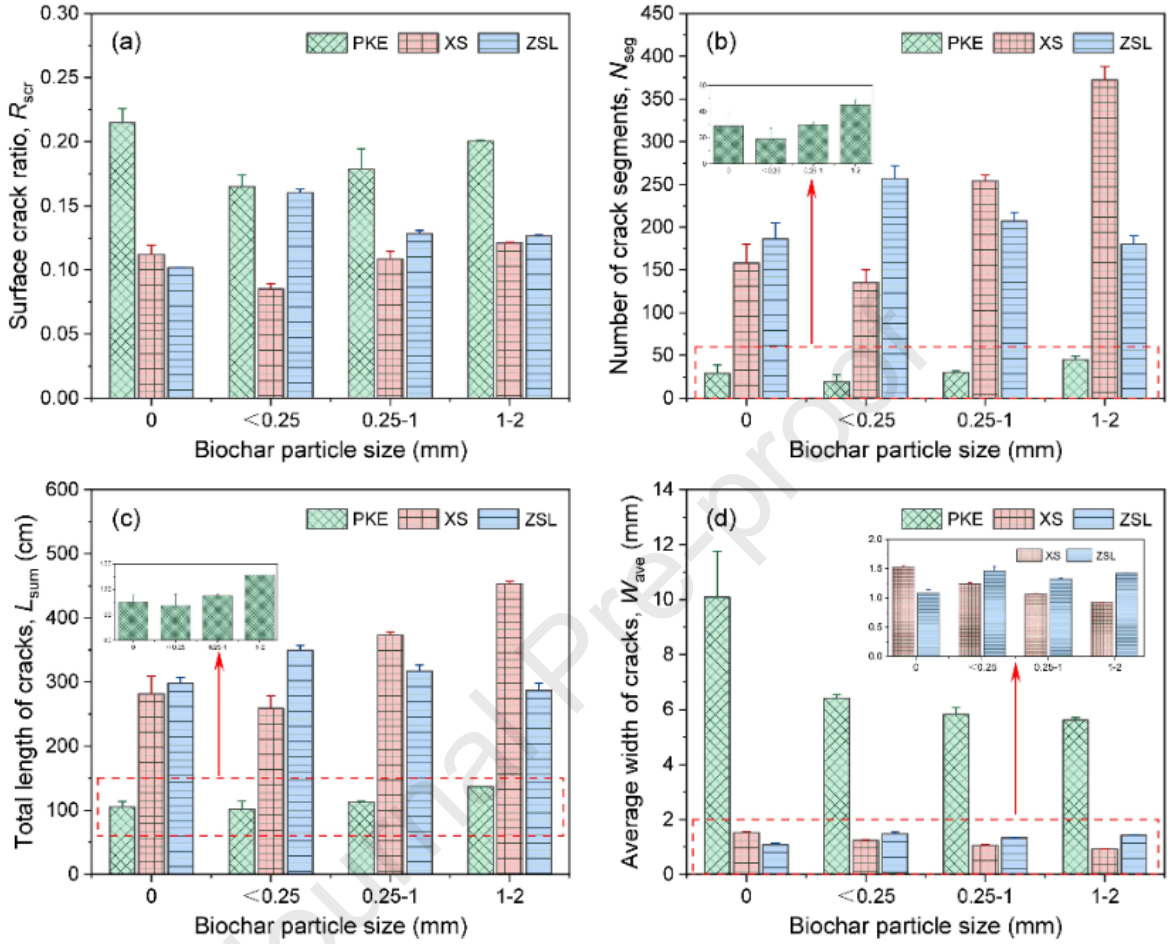

Fig. 11. Quantitative crack parameters of soils with varying biochar particle sizes: (a) Surface crack ratio, R_{scr}; (b) Number of crack segments, N_{seg}; (c) Total length of cracks, L_{sum}; and (d) Average width of cracks, W_{ave}.

The distinct responses of PKE, XS, and ZSL to biochar particle size can be attributed to the different mechanisms involved. As the biochar particle size increases, the direct replacement effect remains constant. However, the direct barrier effect of the biochar diminishes due to the reduction in the exposed surface area, which is not conducive to crack mitigation. Concerning the indirect physical effect, for CPKE3, clear boundary lines were observed between the biochar and clay particles, which led to the disappearance of the close contact in FPKE3 (Figs. 6 and 12a). This loose contact allowed macropores to develop in the soil and eventually a bimodal pore size curve emerged (Fig. 12c). This explains the altered process of crack initiation and propagation, the increase in crack parameters such as R_{scr}, N_{seg}, and L_{sum}, and the decrease in W_{ave} in the coarse biochar-amended PKE. Similar boundary lines were also found in CXS3 (Fig. 12b). Although coarse biochar failed to change the unimodal PSD curve in FXS3, it did cause the curve to shift flat to the right, with an increased pore size (Fig. 12d). This alteration provides more locations

of stress concentration in the soil, which consequently aggravates cracking. Therefore, both the direct barrier and indirect physical effects were responsible for the exacerbated cracking with increasing biochar particle size.

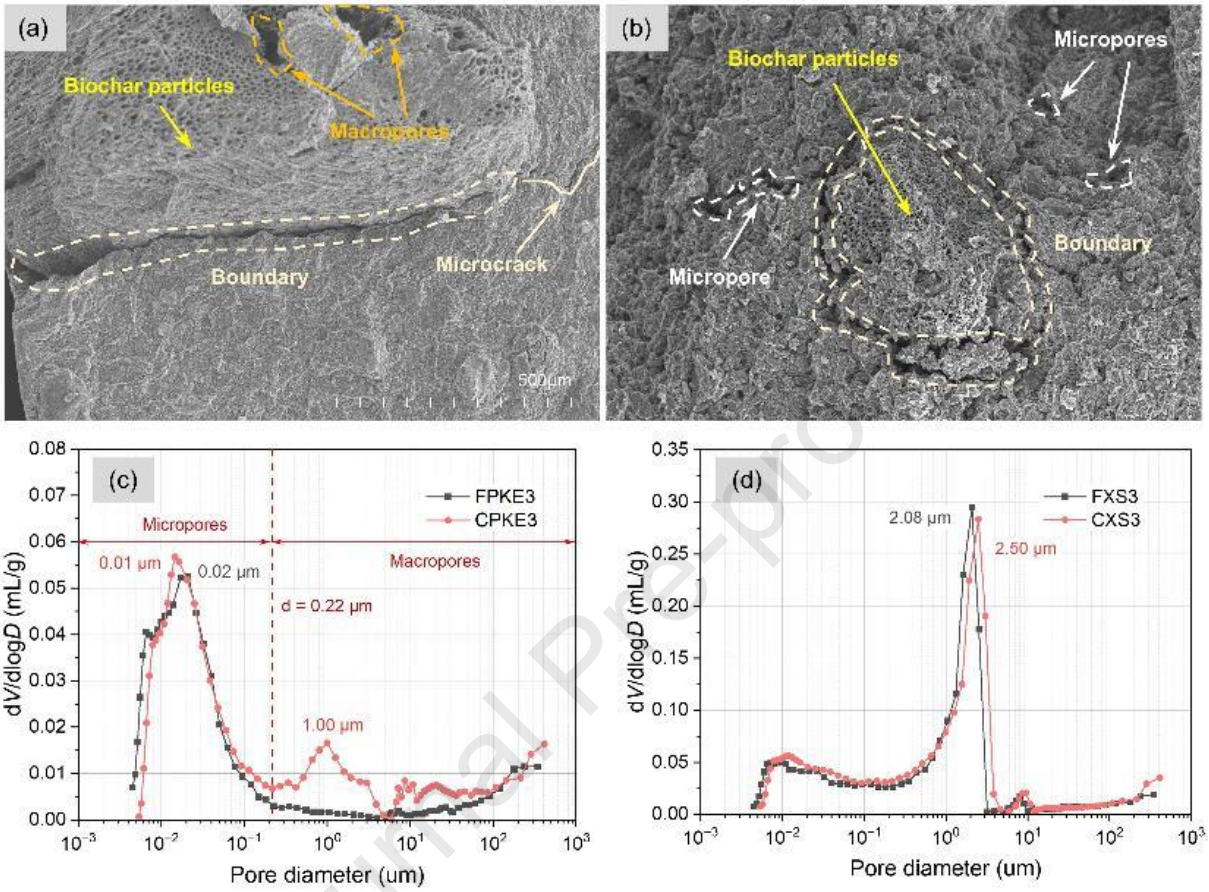

Fig. 12. SEM images of the BAS: (a) CPKE3; and (b) CXS3; and PSD curves of BAS: (c) PKE; and (d) XS.

In contrast, for ZSL, the indirect chemical effect of biochar dominates. Coarse biochar has a lower CEC compared to fine biochar (Reddy et al., 2015; Shen et al., 2015), which results in a reduction in ion exchange capability between biochar and clay particles. The reduction in the bound water film around clay particles resulted in a decreasing trend in crack parameters with increasing biochar particle size, but they were still higher than those of bare ZSL (Fig. 11). Therefore, the effect of biochar particle size should not be ignored when utilizing biochar to modify the desiccation cracking behavior of the soil. To minimize soil cracking and prevent its induced deterioration of engineering properties, it is recommended to use biochar with fine particle size in XS and ZSL.

3.4. Effect of biochar–water–soil interactions on soil cracking

According to the above phenomena and explanations, and on the basis of the previous studies (Lu et al., 2023), we further distinguished the interactions between biochar, water, and soil into direct and indirect effects, as shown in Fig. 13a. The direct effects were achieved by partially

replacing soil particles with biochar (Lu et al., 2022, replacement effect), as well as the barrier effect caused by biochar (Fig. 13c), where negatively charged biochar particles are embedded in soil aggregates and clay has partially filled the pore of biochar, as evidenced by SEM images (Yang et al., 2016; Zhang et al., 2020; Lu et al., 2021). Consequently, the direct effects of biochar can benefit the soil by enhancing its resistance to cracking. The indirect effects can be divided into two categories: physical and chemical. The indirect physical effect was evidenced by alterations to the pore structure of BAS (Fig. 13d). Conversely, the indirect chemical effect of biochar can be attributed to its capacity to modify the bound water film surrounding clay particles by altering the nature of the pore water, including its pH, CEC, and ionic composition (Fig. 13e). The indirect effects of biochar on soil cracking may either inhibit or promote this process, depending on the properties of the biochar and soils. The final macroscopic effect of biochar on soil cracking is the result of a combination of direct and indirect effects (Fig. 13b).

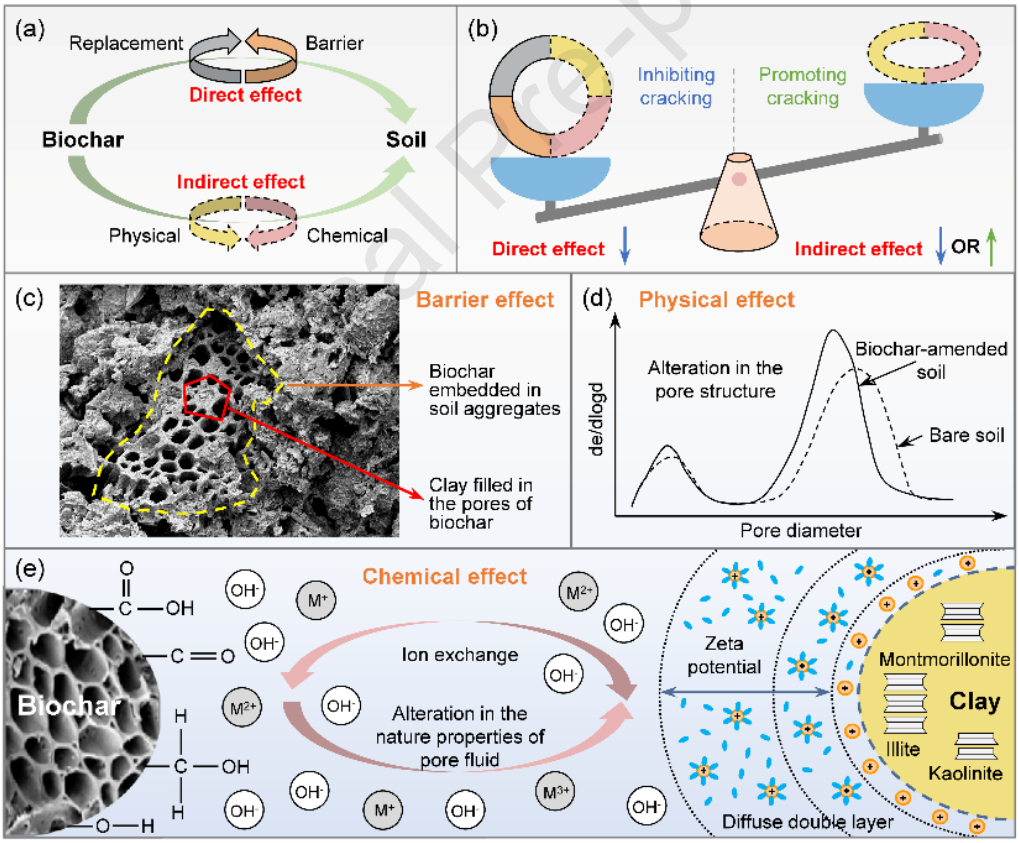

Fig. 13. Schematic of biochar–water–soil interactions.

Although some studies have proposed that the increased water retention of BAS is the main cause of cracking mitigation (Bordoloi et al., 2018; Hussain et al., 2020), biochar itself contains a significant amount of water (e.g. 22.3% in silt loam) (Nakhli and Imhoff, 2020), which may exhibit distinct properties from soil particles during drying. A review of the literature on the effect of biochar on soil cracking by Lu et al. (2023) revealed that the mitigation of cracking in

BAS was not always accompanied by a decrease in the plasticity index. On the contrary, the plasticity index of the soil may either decrease, increase, or remain unchanged, as water gain or loss does not induce volume deformation of biochar. It is the change in the thickness of the bound water film surrounding clay particles after the incorporation of biochar that affects soil cracking, which is defined here as the indirect chemical effect of biochar. An increase in the thickness of the bound water film resulting from the addition of biochar has the potential to aggravate soil cracking, as well as decrease soil strength, and increase soil compressibility. Therefore, when utilizing biochar in subtropical regions, it is imperative to give due consideration to the chemical interactions between biochar and clay particles.

3.5. Significance and limitation

This study provides a comprehensive and detailed analysis of the interaction between biochar and soil in the presence of water, with a particular focus on its impact on the desiccation cracking behavior of three typical soils in subtropical regions. In contrast to previous studies (Bordoloi et al., 2018; Zhang et al., 2020; Yang et al., 2021), our research reveals that biochar can also contribute to the promotion of cracking in certain soils by increasing the bound water film surrounding clay particles. Among these, the primary cause is ion exchange between biochar and clay particles. Due to the significant presence of low-valent cations (e.g. K^+, Ca^{2+}, Na^+, and Mg^{2+}) in biochar (Lu et al., 2023), it is inadvisable to add biochar to soils that are dominated by high-valent cations (e.g. Al^{3+} and Fe^{3+}) in clay minerals. This is particularly pertinent in cases such as lateritic soil, which contains Al^{3+}-based kaolinite as the primary clay mineral due to intense chemical weathering. Conversely, for clay minerals composed of monovalent cations, such as sodium bentonite, biochar has the potential to decrease the bound water film around clay particles and enhance their engineering properties. Situations falling between these extremes will result from a combination of effects, influenced by the ion concentrations and types of biochar and soil, among other factors. This study demonstrates that biochar reduces and insignificantly alters the plasticity index of PKE and XS, where illite is the primary clay mineral. These findings provide guidance for the potential use of biochar in subtropical regions. The implications of this study can extend to a range of geotechnical and geoenvironmental engineering applications, including the utilization of biochar as barrier layers for landfill final covers and as topsoil for both bare and vegetated slopes.

In the field context, the microstructure and macrostructure of the system under investigation, which is a remolded slurry with a homogeneous state, differs from that of undisturbed soils, which exhibit an inhomogeneous pore structure resulting from shrink-swell cycling (DeCarlo and Shokri, 2014). Nevertheless, the presence of similar direct replacement and indirect

chemical effects of biochar on soils in both systems permits a comparison of the impact of biochar on desiccation cracking behavior. Moreover, although the experimental results presented here offer compelling evidence that the addition of biochar significantly alters the cracking behavior of three clayey soils to varying degrees, it is important to recognize that these findings are confined to laboratory conditions and may not fully represent field conditions. Factors such as sample size (e.g. sample dimension and layer thickness) and boundary effects (e.g. basal roughness and friction) may affect the cracking morphology in a different manner in the field. Therefore, field trials are imperative to assess the efficacy of biochar in practical engineering applications.

4. Conclusions

In this study, the biochar–water–soil interactions influencing soil cracking are classified as direct or indirect based on the microstructural analysis. The direct effects of biochar include replacement and barrier effects, while the indirect effects involve changes to pore structure (physical effect) and ion exchange, which affect the bound water film around clay particles (chemical effect). These interactions give rise to contrasting outcomes in soil cracking behavior, where the initial mineral composition and cation type of the soil play a crucial role. It is inadvisable to add biochar to soils that are dominated by high-valent ions (e.g., Al^{3+} and Fe^{3+}) in clay minerals, as this can aggravate soil cracking due to the predominance of the indirect chemical effect over other effects. Conversely, biochar, particularly when of fine particle size, is recommended for crack prevention in soils containing high levels of low-valent cations with montmorillonite and illite as the main clay minerals, where the direct inhibitory effect of biochar prevails. However, high biochar dosages, while yielding better performance, are also accompanied by higher costs, which need to be balanced before considering large-scale field applications of biochar in subtropical regions.

Declaration of Competing Interest

The authors declare that they have no known competing financial interests or personal relationships that could have appeared to influence the work reported in this paper.

Acknowledgments

This research was financially supported by the National Natural Science Foundation of China (Grant Nos. 42277124), the National Key Research & Development Program of China (Grant Nos. 2020YFC1808004), and the Jiangsu Province 333 Talents Youth Talent Support Project.

References

Albrecht, B.A., Benson, C.H., 2001. Effect of desiccation on compacted natural clays. J. Geotech. Geoenviron. Eng. 127 (1), 67–75.

ASTM D–2487, 2017. Standard practice for classification of soils for engineering purposes (Unified Soil Classification System). ASTM International, West Conshohocken, USA.

Bai, W., Zhang, W., Kong, L., Fan, H., Guo, A., Xu, G., 2023. Effect of soaking time of dithionite–citrate–bicarbonate solution on strength and deformation characteristics of lateritic soil. J. Rock Mech. Geotech. Eng. 15 (11), 3039–3049.

Blanco-Canqui, H., 2021. Does biochar application alleviate soil compaction? Review and data synthesis. Geoderma 404, 115317.

Bordoloi, S., Garg, A., Sreedeep, S., Lin, P., Mei, G., 2018. Investigation of cracking and water availability of soil-biochar composite synthesized from invasive weed water hyacinth. Bioresour. Technol. 263, 665–677.

Cheng, Q., Tang, C.S., Xu, D., Zeng, H., Shi, B., 2021. Water infiltration in a cracked soil considering effect of drying-wetting cycles. J. Hydrol. 593, 125640.

Cheng, Q., Tang, C.S., Zeng, H., Zhu, C., An, N., Shi, B., 2020. Effects of microstructure on desiccation cracking of a compacted soil. Eng. Geol. 265, 105418.

Costa, S., Kodikara, J.K., Shannon, B., 2013. Salient factors controlling desiccation cracking of clay in laboratory experiments. Geotechnique 63 (1), 18–29.

Cui, Y., 2022. Soil–atmosphere interaction in earth structures. J. Rock Mech. Geotech. Eng. 14 (1), 35–49.

DeCarlo, K.F., Shokri, N., 2014. Salinity effects on cracking morphology and dynamics in 3-D desiccating clays. Water Resour. Res. 50 (4), 3052–3072.

Delage, P., Audiguier, M., Cui, Y.J., Howat, M.D., 1996. Microstructure of a compacted silt. Can. Geotech. J. 33 (1), 150–158.

D'Angelo, B., Bruand, A., Qin, J., et al., 2014. Origin of the high sensitivity of Chinese red clay soils to drought: significance of the clay characteristics. Geoderma 223, 46–53.

Garg, A., Huang, H., Cai, W., et al., 2021. Influence of soil density on gas permeability and water retention in soils amended with in-house produced biochar. J. Rock Mech. Geotech. Eng. 13 (3), 593–602.

Gu, K., Tang, C., Shi, B., Hong, J., Jin, F., 2014. A study of the effect of temperature on the structural strength of a clayey soil using a micropenetrometer. Bull. Eng. Geol. Environ. 73, 747–758.

Guo, H., Wai, N.C.W., Ni, J., Zhang, Q., Wang, Y., 2024. Three-year field study on grass growth and soil hydrological properties in biochar-amended soil. J. Rock Mech. Geotech. Eng. 16 (7), 2764–2774.

He, Z., Zhang, M., Wilson, M.J., 2004. Distribution and classification of red soils in China. In: Wilson, M.J., He, Z., Yang, X. (Eds), The red soils of China. Springer, Dordrecht, UK. p. 29–33.

Hu, X.F., Wei, J., Du, Y., et al., 2010. Regional distribution of the Quaternary Red Clay with aeolian dust characteristics in subtropical China and its paleoclimatic implications. Geoderma 159 (3–4), 317–334.

Hussain, R., Bordoloi, S., Gupta, P., et al., 2020. Effect of biochar type on infiltration, water retention and desiccation crack potential of a silty sand. Biochar 2, 465–478.

Jien, S.H., Wang, C.S., 2013. Effects of biochar on soil properties and erosion potential in a highly weathered soil. Catena 110, 225–233.

Kumar, H., Cai, W., Lai, J., et al., 2020. Influence of in-house produced biochars on cracks and retained water during drying-wetting cycles: Comparison between conventional plant, animal, and nano-biochars. J. Soils Sediments 20, 1983–1996.

Laird, D., Fleming, P., Wang, B., Horton, R., Karlen, D., 2010. Biochar impact on nutrient leaching from a Midwestern agricultural soil. Geoderma 158 (3–4), 436–442.

Lehmann, J., Cowie, A., Masiello, C.A., et al., 2021. Biochar in climate change mitigation. Nat. Geosci. 14 (12), 883–892.

Liu, C., Tang, C.S., Shi, B., Suo, W.B., 2013. Automatic quantification of crack patterns by image processing. Comput. Geosci. 57, 77–80.

Lu, N., 2020. Unsaturated soil mechanics: Fundamental challenges, breakthroughs, and opportunities. J. Geotech. Geoenviron. Eng. 146 (5), 02520001.

Lu, S.G., Sun, F.F., Zong, Y.T., 2014. Effect of rice husk biochar and coal fly ash on some physical properties of expansive clayey soil (Vertisol). Catena 114, 37–44.

Lu, Y., Gu, K., Shen, Z., Tang, C.S., Shi, B., Zhou, Q., 2023. Biochar implications for the engineering properties of soils: A review. Sci. Total Environ. 164185.

Lu, Y., Gu, K., Shen, Z., et al., 2022. Effects of biochar particle size and dosage on the desiccation cracking behavior of a silty clay. Sci. Total Environ. 837, 155788.

Lu, Y., Gu, K., Zhang, Y., Tang, C., Shen, Z., Shi, B., 2021. Impact of biochar on the desiccation cracking behavior of silty clay and its mechanisms. Sci. Total Environ. 794, 148608.

Meehl, G.A., Tebaldi, C., 2004. More intense, more frequent, and longer lasting heatwaves in the 21st century. Science 305, 994–997.

Morris, P.H., Graham, J., Williams, D.J., 1992. Cracking in drying soils. Can. Geotech. J. 29 (2), 263–277.

Nakhli, S.A.A., Imhoff, P.T., 2020. Models for predicting water retention in pyrogenic carbon (biochar) and biochar-amended soil at low water contents. Water Resour. Res. 56 (11), e2020WR027726.

Peron, H., Hueckel, T., Laloui, L., Hu, L., 2009. Fundamentals of desiccation cracking of fine-grained soils: experimental characterisation and mechanisms identification. Can. Geotech. J. 46 (10), 1177–1201.

Piao, S.L., Ciais, P., Huang, Y., et al., 2010. The impacts of climate change on water resources and agriculture in China. Nature 467 (7311), 43–51.

Pierozan, R.C., Araújo, G.L.S., Palmeira, E.M., Romanel, C., 2023. Influence of variables related to soil weathering on the geomechanical performance of tropical soils. J. Geotech. Geoenviron. Eng. 15 (9), 2423–2440.

Puspanathan, T.K., Jayawardane, V.S., Paul, S.C., Ying, K.S., Shukla, S.K., Anggraini, V., 2022. Effect of biochar on desiccation of marine soils under constant and cyclic temperatures. Acta Geotech. 17, 5441–5464.

Reddy, K.R., Yaghoubi, P., Yukselen-Aksoy, Y., 2015. Effects of biochar amendment on geotechnical properties of landfill cover soil. Waste Manage. Res. 33 (6), 524–532.

Shen, Z., Jin, F., Wang, F., McMillan, O., Al-Tabbaa, A., 2015. Sorption of lead by Salisbury biochar produced from British broadleaf hardwood. Bioresour. Technol. 193, 553–556.

Shen, Z., Zhang, Z., Zhang, M., Rinklebe, J., Ma, Y., Hou, D., 2021. Effect of production temperature and particle size of rice husk biochar on mercury immobilization and erosion prevention of a mercury contaminated soil. J. Hazard. Mater. 420, 126646.

Sherwood, S., Fu, Q., 2014. A drier future? Science 343 (6172), 737–739.

Shi, B., Jiang, H., Liu, Z., Fang, H.Y., 2002. Engineering geological characteristics of expansive soils in China. Eng. Geol. 67 (1–2), 63–71.

Shin, H., Santamarina, J.C., 2011. Desiccation cracks in saturated fine-grained soils: particle-level phenomena and effective-stress analysis. Geotechnique 61 (11), 961–972.

Tang, C.S., Cheng, Q., Leng, T., Shi, B., Zeng, H., Inyang, H.I., 2020. Effects of wetting-drying cycles and desiccation cracks on mechanical behavior of an unsaturated soil. Catena 194, 104721.

Tang, C.S., Cui, Y.J., Tang, A.M., Shi, B., 2010. Experiment evidence on the temperature dependence of desiccation cracking behavior of clayey soils. Eng. Geol. 114 (3–4), 261–266.

Tang, C., Shi, B., Liu, C., Zhao, L., Wang, B., 2008. Influencing factors of geometrical structure of surface shrinkage cracks in clayey soils. Eng. Geol. 101 (3–4), 204–217.

Tang, C.S., Zhu, C., Leng, T., Shi, B., Cheng, Q., Zeng, H., 2019. Three-dimensional characterization of desiccation cracking behavior of compacted clayey soil using X-ray computed tomography. Eng. Geol. 255, 1–10.

Tian, B.G., Cheng, Q., Tang, C.S., Zeng, H., Xu, J.J., Shi, B., 2022. Effects of compaction state on desiccation cracking behaviour of a clayey soil subjected to wetting-drying cycles. Eng. Geol. 302, 106650.

Wan, Y., Dong, Z., He, X., et al., 2022. Effect of biochar on permeability of compacted soil and its microscopic mechanism. Can. Geotech. J. 59 (12), 2184–2195.

Wong, J.T.F., Chen, Z., Wong, A.Y.Y., Ng, C.W.W., Wong, M.H., 2018. Effects of biochar on hydraulic conductivity of compacted kaolin clay. Environ. Pollut. 234, 468–472.

Woolf, D., Amonette, J.E., Street-Perrott, F.A., Lehmann, J., Joseph, S., 2010. Sustainable biochar to mitigate global climate change. Nat. Commun. 1 (1), 56.

Xu, R., Zhao, A., Li, Q., Kong, X., Ji, G., 2003. Acidity regime of the Red Soils in a subtropical region of southern China under field conditions. Geoderma 115 (1–2), 75–84.

Yan, C., Wang, T., Ke, W., Wang, G., 2021. A 2D FDEM-based moisture diffusion–fracture coupling model for simulating soil desiccation cracking. Acta Geotech. 16, 2609–2628.

Yan, M., Sun, C., Xu, J., Dong, J., Ke, W., 2014. Role of Fe oxides in corrosion of pipeline steel in a red clay soil. Corrosion Sci. 80, 309–317.

Yang, B., Li, D., Yuan, S., Jin, L., 2021. Role of biochar from corn straw in influencing crack propagation and evaporation in sodic soils. Catena 204, 105457.

Yang, C.D., Lu, S.G., 2021. Effects of five different biochars on aggregation, water retention and mechanical properties of paddy soil: A field experiment of three-season crops. Soil Till. Res. 205, 104798.

Yang, F., Zhao, L., Gao, B., Xu, X., Cao, X., 2016. The interfacial behavior between biochar and soil minerals and its effect on biochar stability. Environ. Sci. Technol. 50 (5), 2264–2271.

Zhang, Y., Gu, K., Li, J., Tang, C., Shen, Z., Shi, B., 2020. Effect of biochar on desiccation cracking characteristics of clayey soils. Geoderma 364, 114182.

Zhang, Y., Huang, Y., Wang, Z., et al., 2024. A quantitative study on the characteristics of desiccation cracks and their effect on the shear failure characteristics of granite red soil. Bull. Eng. Geol. Environ. 83 (1), 27.

	**Dr. Kai Gu** is now a full professor in Engineering Geology at the School of Earth Sciences and Engineering, Nanjing University, China. He obtained his BSc and PhD degrees from Nanjing University in 2009 and 2014, respectively. He was a visiting scholar at the University of Cambridge from 2012 to 2013. His expertise includes multi-physics field monitoring with fiber-optic technology, shallow geothermal energy, and geoenvironmental engineering using sustainable materials. He has presided over 16 projects and published more than 90 peer-reviewed papers. He is the Vice-Secretary General of the International Society of Environmental Geotechnology (ISEG).

Declaration of interests

☒ The authors declare that they have no known competing financial interests or personal relationships that could have appeared to influence the work reported in this paper.

☐The authors declare the following financial interests/personal relationships which may be considered as potential competing interests: